Surface Impedance Measurements of Single Crystal MgB_2 Films for Radiofrequency Superconductivity Applications

B. P. Xiao,[1,2] X. Zhao,[1] J. Spradlin,[1] C. E. Reece,[1, a)] M. J. Kelley,[1,2] T. Tan,[3] and X. X. Xi[3]

[1]*Thomas Jefferson National Accelerator Facility, Newport News, VA 23606, U.S.A.*

[2]*Applied Science Department, College of William and Mary, Williamsburg, VA 23187, U.S.A.*

[3]*Department of Physics, Temple University, Philadelphia, PA 19122, U.S.A.*

We report microstructure analyses and superconducting radiofrequency (SRF) measurements of large scale epitaxial MgB_2 films. MgB_2 films on 5 cm dia. sapphire disks were fabricated by a Hybrid Physical Chemical Vapor Deposition (HPCVD) technique. The electron-beam backscattering diffraction (EBSD) results suggest that the film is a single crystal complying with a $MgB_2(0001)//Al_2O_3(0001)$ epitaxial relationship. The SRF properties of different film thicknesses (200 nm and 350 nm) were evaluated under different temperatures and applied fields at 7.4 GHz. A surface resistance of 9±2 μΩ has been observed at 2.2 K.

SRF accelerating cavities for particle accelerators made from bulk niobium (Nb) materials are the state-of-art facilities for exploring frontier physics, such as Continuous Electron Beam Accelerator Facility (CEBAF), European X-Ray Laser Project (XFEL), Facility for Rare Isotope Beams (FRIB), Spallation Neutron Source (SNS) and the proposed International Linear Collider (ILC). The maximum accelerating gradient of Nb SRF resonant cavities has been pushed to 52 MV/m for a single-cell cavity with quality factor higher than 10^{10} at 1.3 GHz and 2 K temperature [1], approaching the theoretical limit of Nb. Superconductors with surface resistance lower than, and superheating critical field higher than, those of Nb are of great interest for SRF applications. Magnesium diboride (MgB_2), discovered to be a superconductor by Nagamatsu et al in 2001 [2], is under investigation for possible future use in SRF applications.

MgB_2 is a binary compound that contains boron (B) layers separated by hexagonal close-packed magnesium (Mg) layers, with a high critical temperature around 39~40 K [3], twice as high as the next highest binary superconductor's T_c (Nb_3Ge at 23 K), which suggests possi-

a) Electronic mail: reece@jlab.org

ble applications at temperatures higher than 2 K, the current typical operation temperature of Nb cavities. MgB_2 has two energy gaps, with a π-band at 2.3 meV and a σ-band at 7.1 meV [4]. At a temperature much lower than its critical temperature, the BCS surface resistance $R_s \sim (A\omega^2/T)exp(-\Delta/k_bT)$ is dominated by the π-band. The BCS surface resistance of MgB_2 could potentially be much lower than that of Nb considering that Nb's energy gap is 1.5 meV. The coherence length of MgB_2 is about 5 nm. Experiments reveal that the grain boundaries of MgB_2 do exhibit suppression of supercurrent density [5, 6] in DC applications. However, in SRF applications, a MgB_2 film with large grain size is preferred because grain boundaries in the film could cause strong pinning, which would lead to high field Q drop [7]. RF penetration depth is one to two hundred nm at temperatures below 5 K in applications in the GHz range. To shield most of the applied RF field, a film with several hundred nm thickness is preferred, which makes quality control harder. Comparing with Nb, MgB_2 has a smaller lower critical field H_{c1} and a larger upper critical field H_{c2}, which are determined by its penetration depth and coherence length, respectively. The superheating critical field of MgB_2, calculated from $H_{sh} = 0.75\sqrt{H_{c1}H_{c2}}$ [8, 9], is 170~1000 mT depending on the field's direction [3], which suggests that it might be possible to achieve 200 MV/m gradient [10]. MgB_2 is also an attractive choice for multilayer film coatings to benefit from the lower surface resistance, which was proposed by Gurevich [11].

While past research has largely focused on polycrystalline MgB_2 [12], this study was initiated to reveal a relationship between thickness and SRF performance of single crystal MgB_2. High quality MgB_2 films were grown epitaxially on *C*-plane sapphire substrates, $Al_2O_3(0001)$, with a HPCVD technique [13, 14] and was characterized by EBSD with Pole Figures (PFs) for microstructure. We conducted a novel surface impedance characterization (SIC) [15, 16] for films with 200 nm and 350 nm thickness. The SIC testing of SRF properties was set at 7.4 GHz, under different temperatures and applied fields with higher resolution than previous works [17-19].

The principle of the HPCVD system was described in reference [13, 14]. The system has been modified to accommodate 5 cm substrate for potential SRF application. The system was pumped down below 10^{-2} Torr. Then UHP hydrogen was introduced to flush the system. Deposition was conducted in a hydrogen atmosphere of 40 Torr to prevent oxidation. The substrate, along with magnesium pellets placed nearby on the substrate heater, was heated to 750 ℃, when the magnesium pellets melted and a high Mg vapor pressure was generated near the substrate. A flow of 40 sccm diborane gas mixture (5% concentration in hydrogen) was then introduced. Diborane decomposed in the hot space near the substrate heater to provide active boron atoms, which reacted with magnesium vapor to form MgB_2 and deposit on the substrate.

Three 5 cm dia. samples have been fabricated for SRF property characterization, with two at 200 nm thickness (labeled as MgB_2-200-I and MgB_2-200-II) and one at 350 nm thickness (labeled as MgB_2-350). Small samples with 1×1 cm^2 size and 350 nm thickness have been fabricated for surface characterization.

In previous studies [13, 14], XRD Bragg-Brentano survey (θ-2θ scan), and φ-scan on the MgB_2 {1,1,-2,0} crystals plane were conducted to reveal the films' microstructure. Those XRD survey suggested that the MgB_2 films had epitaxially grown on SiC or *C*-plane sapphire crystals. The epitaxial relationship complies with crystallographic relationship: $MgB_2(0001)$// SiC(0001) or Al_2O_3 (0001).

Besides utilizing XRD, which probes a depth of about one micron, Electron backscattering diffraction (EBSD) technique was used in this work to investigate microstructure of the films' topmost layer, in depth of 40 nm, to ensure that the collected information comes from the MgB_2 film only and contains no information from substrate. The EBSD system applied in this study that made by EDAX-TSL™ company is installed on an Amray™ SEM. The EBSD setup is equipped with TSL-OIM™ software to acquire and index the crystallographic orienta-

tions. Principles of the EBSD technique may be found in Ref. [20]. Utilizing EBSD to characterize MgB_2 crystallites has not been previously reported. Since there is no such phase entry in the OIM Data Collection™ 5.0, we established a new entry of MgB_2 by defining the crystal structure as P6/mmm space symmetry group, with the lattice constants a=0.32 nm and c= 0.39 nm.

Figure 1 is the EBSD data for a MgB_2/*C*-plane sapphire film. The EBSD survey area of 150×150 μm^2 with a 5 μm e-beam step has an average Confident Index (CI) of 0.55. The [Min, Max] CI of the survey is [0.086, 0.74]. The average Image Quality (IQ) of the survey is 997. The IQ, being close to a well-ordered bulk metallic sample after annealing/chemical polishing, indicates that the film's crystal quality is high. Grayscale of the map is rendered by the CI of OIM™, with a grayscale rendering of the CI range [0.1, 0.743]. The entire survey area is rendered in red, which means every pixel is in the (0001) orientation. A hexagon in the figure represents the oriented real lattice.

For three largely-separated survey areas, the average crystallographic misorientation of each survey area is <0.3 degree. The misorientation angle is a conventional parameter to gauge the crystal quality of a grain. Subgrains, strain, polygonizations, or other micro-structure defects will lead to a larger misorientation angle. A misorientation <0.3 degree in an area of 150×150 μm^2 suggests the film is of reasonably good grain quality for SRF applications. Fig 1 c&d are PFs representative of the measurements of all survey areas. The PFs are exactly the same for all three survey areas. The converging of the PFs, along with misorientation plots and IPF figures, all indicates the absence of grain boundaries (>0.3^0) in the MgB_2 film. In addition to using EBSD to deduce the stereographic projection PFs, XRD PF measurements were also conducted to visualize the film's reciprocal lattice space and to study the crystal textures in a larger area (~3 mm^2). Both EBSD and XRD PFs are consistent, demonstrating the MgB_2 are single crystal epitaxial films with a grain size only limited by substrate dimension at 1×1 cm^2, following the epitaxial relationship $MgB_2(0001)$// $Al_2O_3(0001)$.

EDX and SEM have been placed to examine the chemical composition and surface morphology of the films. The atomic percentage ratios of Mg vs. B is approximately 1:2 with a ±10% error. The film's outer most surface has a fairly flat but unique growth topography, which has been reported in Ref. [13].

The MgB_2 sample has been put at the open end of a TE_{011} cylindrical Nb cavity with a sapphire rod inside, described in [15, 16]. The system provides a resonant field at 7.4 GHz. The cavity body is surrounded by liquid helium during the test and the sample is thermally isolated from it, which differs from the previous measurements [17-19] by making the RF effect on sample the only contribution to the induced heat and resonance frequency change. Heat can be conducted from the sample only via the calorimeter. The effective surface impedance of the sample can be derived by directly substituting heater heat for RF heat under controlled RF field and temperature conditions. This system could detect as low as 1 μW power applied on the sample/sample holder, enabling the resolution of surface resistance as low as 1.2 nΩ at 5 mT peak magnetic field.

The effective surface impedance can be calculated from formula:

$$Z_{eff} = \frac{P_{rf}}{kH_{pk}^{\ 2}} + i\omega\mu_0(\lambda_{ref} + \frac{f - f_{ref}}{M})$$

The real part is the effective surface resistance and imaginary part is the effective surface reactance. P_{rf} is the RF induced heat, k and M are geometry dependent coefficients and ω is the resonant circular frequency. The RF induced heat is calculated from the difference between the power from the heater required to keep a constant sample temperature without RF fields in the cavity and the power from the heater re-

quired to keep the sample's equilibrium temperature unchanged when RF fields are present, so called power compensation technique. The change of effective surface reactance is proportional to the change of effective penetration depth. It can be derived from changes of the resonant frequency of the TE_{011} mode versus sample temperature.

The transition temperature can be measured from the loaded quality factor change while changing the sample temperature. The transition temperatures of MgB_2-200-I and MgB_2-200-II are both at 39.3±0.2 K, while that of MgB_2-350 is at 39.5±0.2 K.

The penetration depth λ_s is derived from the effective penetration depth using $\lambda_{eff} = \lambda_s \coth(d/\lambda_s)$ [21] with d the film thickness. The results are plotted in Figure 2. The measurement errors of penetration depth and sample temperature are 5% and 0.01 K, respectively. Theoretical value based on BCS theory [22] and Mattis-Bardeen's anomalous skin effect of a superconductor [23] is calculated using a code SRIMP, written by Halbritter [24]. The suggested parameters Δ/kT_c = 1.08, London penetration depth = 180 nm, coherence length = 6 nm, mean free path = 38 nm have been achieved using a fitting code written by Ciovati [25].

The effective surface resistance of the samples was measured at temperatures between 2.1 K and 40 K, with peak fields between 0.6mT and 3.7mT, at 7.4GHz, shown in Figure 3. The surface resistance of a large grain Nb sample with 1:1:2 buffered chemical polish (BCP) solution of HF (49% wt), HNO_3 (69% wt), and H_3PO_4 (85% wt) at room temperature, measured using the same apparatus, is plotted as a reference. At temperatures above 4 K, the MgB_2-350 sample has a lower surface resistance than Nb. At 2.2 K, the effective surface resistance decreased from 20 μΩ to 9 μΩ with the film thickness increase from 200 nm to 350 nm. The lowest effective surface resistance measured is 9±2 μΩ at 2.2 K, which is consistent with the previous best reported results [19, 26, 27] using the f^2 rule for normalization [19, 26], with much smaller systematic errors. We note that the 350 nm sample is less than two penetration depths thick at low temperatures and much less at higher temperatures. This must be taken into account when interpreting the effective surface resistance with respect to a BCS model. For the MgB_2-350 sample, the effective surface resistance versus magnetic field was measured with fields up to 10 mT at 3 K sample temperature. Results are shown in Figure 4. Effective surface resistance increased from 10 μΩ to 35 μΩ with increased fields from 0.5 mT to 10 mT.

In conclusion, MgB_2 films on 5 cm sapphire disks have been fabricated using the HPCVD technique. EBSD and XRD PFs revealed that these films are single crystal. Surface impedance measurements at 7.4 GHz showed a decreasing effective surface resistance with increasing film thickness, with the lowest value at 9±2 μΩ at 2.2 K. The 350 nm sample exhibited a lower surface resistance than Nb at temperatures above 4 K, and MgB_2's effective surface resistance at 3 K increased 3.5 times with increased fields from 0.5 mT to 10 mT. These non-linear losses clearly merit further investigation. Development of MgB_2 for SRF application will continue.

This work is supported by Jefferson Science Associates, LLC under U.S. DOE Contract No. DE-AC05-06OR23177 and by DOE under Contract No. DE-SC0004410. The U.S. Government retains a non-exclusive, paid-up, irrevocable, world-wide license to publish or reproduce this manuscript for U.S. Government purposes.

[1]R. L. Geng *et al.*, in Proceedings of 2007 Particle Accelerator Conference (Albuquerque, New Mexico, 2007), p. 2337.

[2]J. Nagamatsu *et al.*, Nature **410**, 63 (2001).

[3]C. Buzea, and T. Yamashita, Superconductor Science and Technology **14**, 115 (2001).

[4]M. Iavarone *et al.*, PH YSICA L R EV I EW L ET T ERS **89**, 187002 (2002).

[5]S. B. Samanta *et al.*, PHYSICAL REVIEW B **65**, 092510 (2002).

[6]M. Eisterer, SUPERCONDUCTOR SCIENCE AND TECHNOLOGY **20**, R47 (2007).

[7]A. Gurevich, and G. Ciovati, PHYSICAL REVIEW B **77**, 104501 (2008).

[8]J. K. Hasan Padamsee, Tom Hays, (1998).

[9]G. Catelani, and J. P. Sethna, Physical Review B **78**, 224509 (2008).

[10]E. Hand, Nature **456**, 555 (2008).

[11]A. Gurevich, APPLIED PHYSICS LETTERS **88**, 012511 (2006).

[12]M. Putti *et al.*, Supercond. Sci. Technol. **16**, 188 (2003).

[13]X. ZENG *et al.*, Nature Materials **1**, 35 (2002).

[14]C. Zhuang *et al.*, Supercond. Sci. Technol. **22**, 025002 (2009).

[15]B. P. Xiao *et al.*, in 23rd Particle Accelerator Conference (Vancouver, Canada, 2009), p. 2144.

[16]B. P. Xiao *et al.*, Review of Scientific Instruments **82**, 056104 (2011).

[17]A. G. Zaitsev *et al.*, 7th European Conference on Applied Superconductivity **43**, 309 (2006).

[18]B. B. Jin *et al.*, Physical Review B: Condensed Matter and Materials Physics **66**, 104521 (2001).

[19]N. Klein *et al.*, IEEE TRANSACTIONS ON APPLIED SUPERCONDUCTIVITY **13**, 3253 (2003).

[20]F. J. HUMPHREYS, JOURNAL OF MATERIALS SCIENCE **36**, 3833 (2001).

[21]N. Klein *et al.*, J. Appl. Phys. **67**, 6940 (1990).

[22]J. Bardeen, L. N. Cooper, and J. R. Schrieffer, Physical Review **108**, 1175 (1957).

[23]D. C. Mattis, and J. Bardeen, Physical Review **111**, 412 (1958).

[24]J. P. Turneaure, J. Halbritter, and H. A. Schwettman, Journal of Superconductivity **4**, 341 (1991).

[25]G. Ciovati, (Old Dominion University, Norfolk VA, 2005), p. 218.

[26]D. E. Oates, Y. D. Agassi, and B. H. Moeckly, (2007).

[27]A. V. Pogrebnyakov *et al.*, IEEE TRANSACTIONS ON APPLIED SUPERCONDUCTIVITY **17**, 2854 (2007).

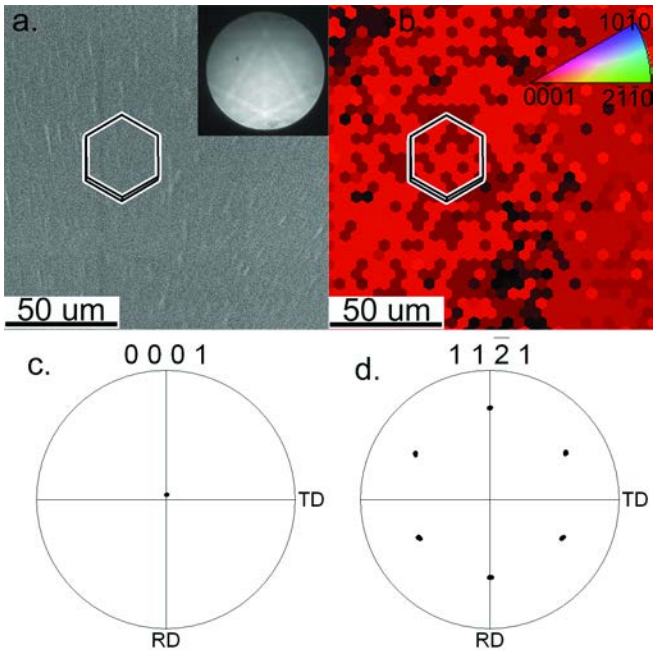

Figure 1. Electron backscattering diffraction (EBSD) results of a MgB_2 film on *C*-plane sapphire. a). a scanning electron micrograph (SEM) of a survey area, the inset at top-right is a representative Kikuchi diffraction image, which shows clear diffraction bands; b). a color-coded inverse pole figure (IPF) of the same area, the inset at top-right is the color-coded crystallographic legend. c). and d). are the PFs being deduced from the EBSD survey in (0001) and (1,1,-2,1) representations respectively.

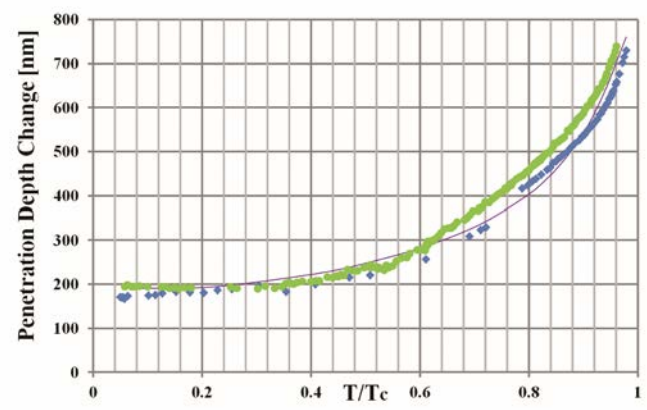

Figure 2. ◆MgB_2-200-I with T_c at 39.3 K ● MgB_2-350 with T_c at 39.5 K Penetration depth versus sample temperature of MgB_2 on sapphire substrate – BCS penetration depth.

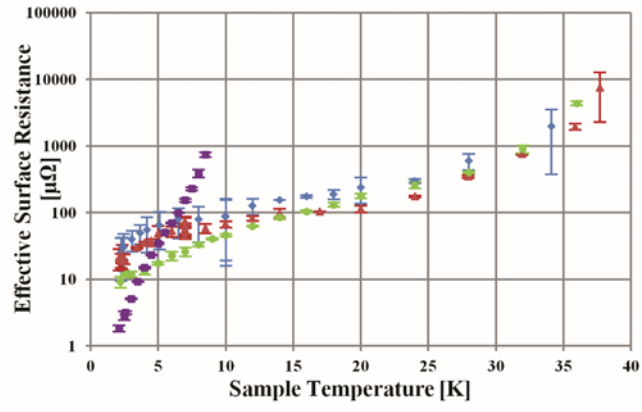

Figure 3. ◆MgB_2-200-I ▲MgB_2-200-II ●MgB_2-350 Effective surface resistance versus sample temperature of MgB_2 on sapphire substrate

■Surface resistance versus sample temperature of large grain Nb sample.

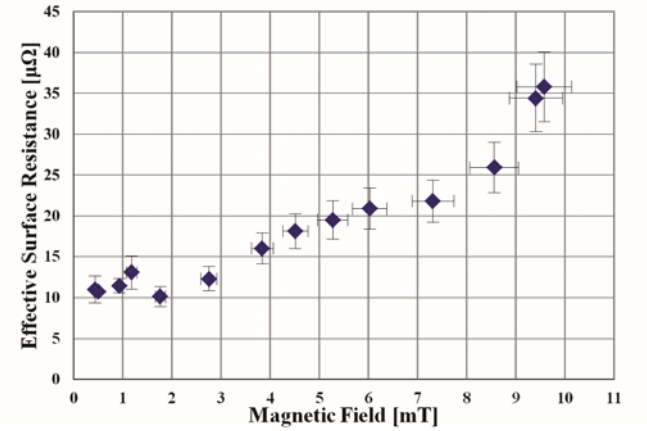

Figure 4. Effective surface resistance versus magnetic field at 3 K sample temperature.